point before the implosion is confined within the range of a few percent of the characteristic length L from a focusing point. Therefore, we may say that the ray shock theory[2] gives a reasonable approximation to the flowfield so far as the flowfield far from the focus is concerned.

Acknowledgments

The first author expresses his sincere thanks to Asako Inoue for her continuous encouragement. The authors express their gratitude to B. E. Milton, University of New South Wales, Australia, for his kind advice and suggestions. Thanks are also due to K. Sawada, Institute of Fluid Science, Tohoku University, for his assistance in this study.

References

[1]Milton, B. E., "The Focusing of Shock Waves in Two-Dimensional and Axi-Symmetric Ducts," *Proceedings of the International Workshop on Shock Wave Focusing,* edited by K. Takayama, Inst. of Fluid Science, Tohoku Univ., Sendai, Japan, 1989, pp. 155–191.

[2]Milton, B. E., "Mach Reflection Using Ray-Shock Theory," *AIAA Journal,* Vol. 13, No. 11, 1975, pp. 1531–1533.

[3]Leer, B. V., "Flux-Vector Splitting for the Euler Equations," *Proceedings of the 8th International Conference on Numerical Methods in Fluid Dynamics,* Lecture Notes in Physics, Vol. 170, Springer-Verlag, 1982, pp. 507–512.

Wakes of Three Axisymmetric Bodies at Zero Angle of Attack

Özlem İlday,* Hayri Acar,† M. Kubilay Elbay,‡ and Veysel Atli§
Istanbul Technical University, Istanbul, Turkey

Nomenclature

C_D = drag coefficient
d = maximum diameter of the model
l = total length of the model
Re_d = Reynolds number based on maximum body diameter, $U_\infty d/\nu$
r = radial distance from the wake centerline
r_b = r position where $\bar{U}_d = \frac{1}{2}(\bar{U}_d)_{\max}$
U_∞ = freestream velocity
$\bar{U}$ = mean velocity in the x direction
$\bar{U}_d$ = velocity defect, $\bar{U}_{\max} - \bar{U}$
$\sqrt{(u'^2)}$ = rms velocity fluctuations in the x direction
u_0 = $\sqrt{(u'^2)}/U_\infty$
u_1 = $\sqrt{(u_{CL}'^2)}/U_\infty$
u_2 = $\sqrt{(u_{CL}'^2)}/|\bar{U}_{CL}|$
x = distance from the base of the model in the freestream direction
x_{sp} = length of the recirculation region

Subscript
CL = centerline of the wake

Received Oct. 21, 1991; revision received Sept. 6, 1992; accepted for publication Sept. 15, 1992.

*Research Assistant, Aeronautical Engineer, Faculty of Aeronautics and Astronautics, 80626 Maslak.

†Research Assistant, Aeronautical Engineer, Faculty of Aeronautics and Astronautics, 80626 Maslak.

‡Research Assistant, Aeronautical Engineer, Faculty of Aeronautics and Astronautics, 80626 Maslak.

§Associate Professor, Faculty of Aeronautics and Astronautics, 80626 Maslak.

Introduction

THE flow separation aft of a blunt-based axisymmetric body at zero angle of attack creates an axisymmetric wake that is the most complex part of the flowfield. An axisymmetric wake consists of a near-wake region and a far-wake region. The near-wake region exists just after the body base, creating a recirculation region covered by the free-shear layer.

Delery and Siriex[1] and Delery and Lacau[2] outlined the axisymmetric wake physics based on earlier investigations. Merz et al.[3] investigated the effect of Mach number on the turbulent near-wake of a cylindrical blunt-based body over the entire subsonic Mach number range. Merz et al.[4] also experimentally investigated the near wake of an axisymmetric semi-elliptical afterbody. Atli[5] performed some hot-wire measurements to investigate the wakes of four complex bodies of revolution at zero angle of attack. Despite these and other works, new investigations are necessary for more information on the problem because of its fundamental and practical importance. New data may also be useful for comparison with computational predictions of the flowfield.

In the present work the wakes of three axisymmetric missile-type bodies with different afterbody geometry at zero angle of attack and at a low subsonic velocity were studied by using a constant temperature hot-wire anemometer. Mean velocity and turbulence measurements, both along and across the wake, were performed. Turbulence was considered as the time-averaged rms fluctuating velocities. Vortex shedding and instability in the free-shear layer were not treated.

Models and Experimental Technique

The models shown in Fig. 1 have the same fineness ratio, $l/d = 16.4$, with the same tangent-ogive nose and cylindrical main body. The first model has a flared afterbody with a neck, the second one a blunt base, and the third one a truncated conical afterbody (boat-tail). The surfaces of the models were smooth.

All of the tests were conducted at zero angle of attack in an open-circuit, low-speed wind tunnel with a closed test section of 50 × 50 × 200 cm. The freestream velocity U_∞ was 10 m/s ($M_\infty \cong 0.03$) with the freestream turbulence intensity $\sqrt{(u'^2)}/U_\infty = 0.3\%$. The Reynolds number Re_d based on maximum body diameter was 2×10^4. A hot-wire anemometer system of DISA (55M) was used with a personal computer and an Analog/Digital converter of Data Acquisition 380 Validyne. The models were supported from one side by two thin circular stings 5 mm in diameter. The support of the hot-wire probe was placed perpendicular to the model symmetry axis and to the model supports to minimize the effects of the supports. Blockage area ratio was less than 0.3% so that no correction for blockage effects has been made. The positional accuracy of the probe traverse was ±0.1 mm, and the accuracy of the hot-wire anemometer outputs for mean velocity and fluctuations is about ±0.1 and ±0.002 m/s, respectively.

The outputs of a hot-wire anemometer do not indicate the flow direction; in other words, the mean velocity output of the

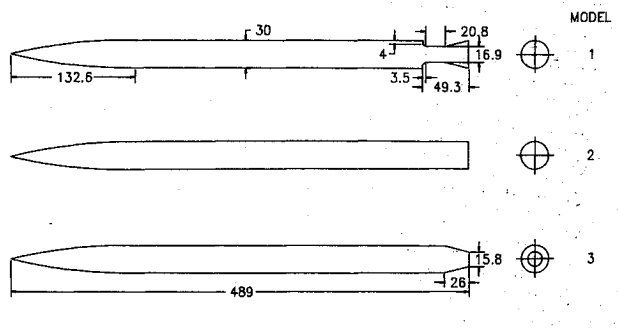

Fig. 1 Model geometries (dimensions in mm).

hot-wire anemometer is always positive. However, the reverse flow in the recirculation region could be identified with an increase, followed by a decrease in the output of the anemometer for the mean velocity when the probe entered the reverse flow region.[6] Therefore, it is necessary to change the sign of the mean velocity output of the anemometer to obtain the true mean velocity profiles in the reverse flow region. This procedure has been used in the present work for the mean velocity profiles of near-wake region.

The drag coefficients of the models were obtained by the momentum equation[7] using the velocity profiles across the wake at the station $x/d = 4$, where the static pressure is approximately equal to the freestream static pressure.

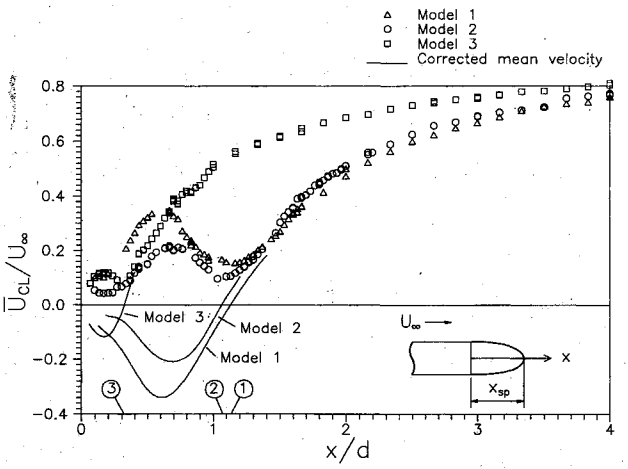

Fig. 2 Mean velocity distribution along the centerline of the wake for all of the models (1, 2, and 3: free-stagnation points for corresponding models).

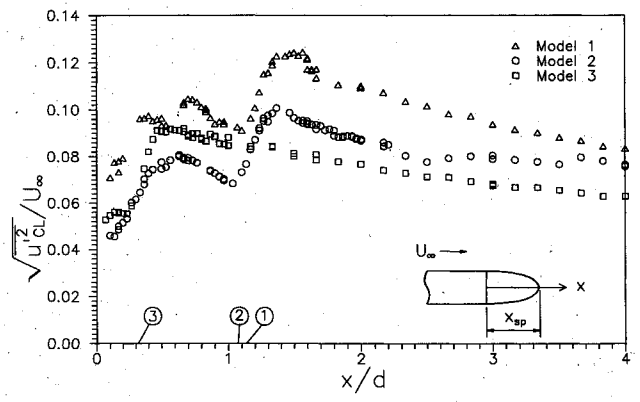

Fig. 3 Longitudinal variations of velocity fluctuations in terms of the freestream velocity on the wake centerline for all of the models (1, 2, and 3: free-stagnation points for corresponding models).

Results and Discussion

As seen in Fig. 2, the reverse flow mean velocity along the centerline of the wake in the recirculation region reaches a maximum value at a distance from the base of about 60% of the length of the recirculation region for all of the models. The length of the recirculation region in terms of the maximum body diameter x_{sp}/d is 1.13 and 1.07 for models 1 and 2, respectively, although it is 0.32 for model 3. The maximum values of $\bar{U}_{CL}/U_\infty$ in the reverse flow are about 0.34, 0.21, and 0.11 for models 1, 2, and 3, respectively.

The velocity fluctuations on the centerline of the wake were expressed in terms of freestream velocity and local mean velocity as $u_1 = \sqrt{(u'^2_{CL})}/U_\infty$ and $u_2 = \sqrt{(u'^2_{CL})}/|\bar{U}_{CL}|$, respectively. The variation of u_1 along the centerline of the wake exhibits two peaks for all of the models, as seen in Fig. 3. The first peak is noted at about the midpoint of the distance between the base and the free-stagnation point. The second peak, which is higher than the first one, takes place just after the free-stagnation point. Figure 3 also shows that the use of a circular cylinder with a constant diameter instead of a flared geometry as an afterbody reduces the turbulence intensity in the wake. This reduction becomes more pronounced with a boat-tail. The variation of u_2 along the centerline of the wake also presents two peaks for each model as seen in Fig. 4. The first peak exists just near the base, and the second one occurs near the free-stagnation point.

The mean velocity and turbulence intensity profiles across the wake are plotted in Figs. 5 and 6, respectively. These figures show that the recirculation region becomes smaller by using a boat-tail type afterbody as indicated before. The maximum of turbulence intensity in the wake is located on a

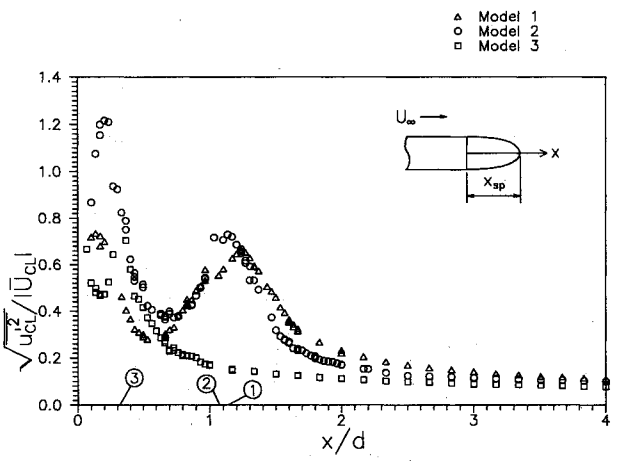

Fig. 4 Longitudinal variations of velocity fluctuations in terms of the local mean velocity on the wake centerline for all of the models (1, 2, and 3: free-stagnation points for corresponding models).

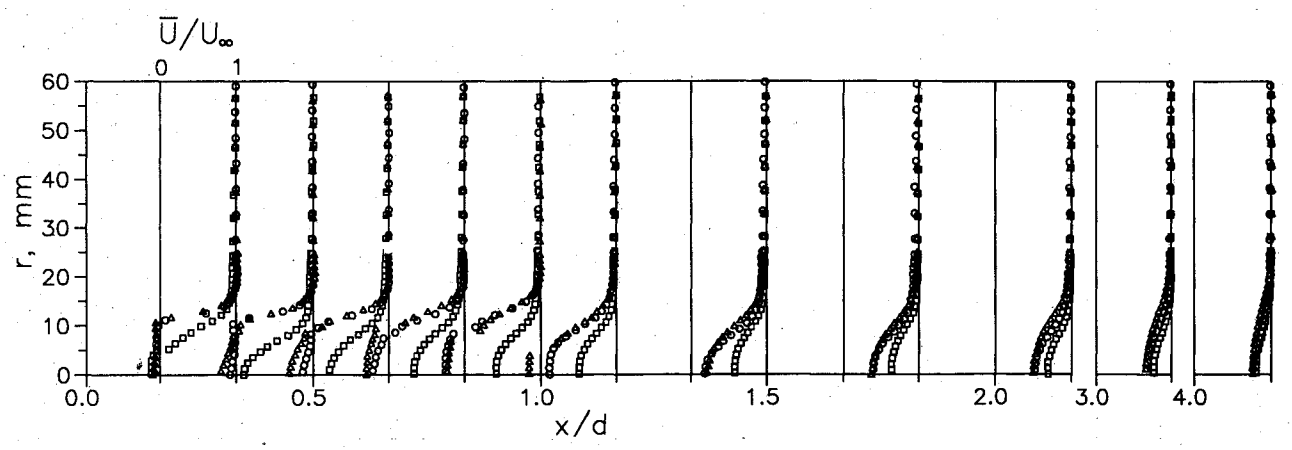

Fig. 5 Mean velocity profiles across the wake (Δ: model 1, ○: model 2, □: model 3).

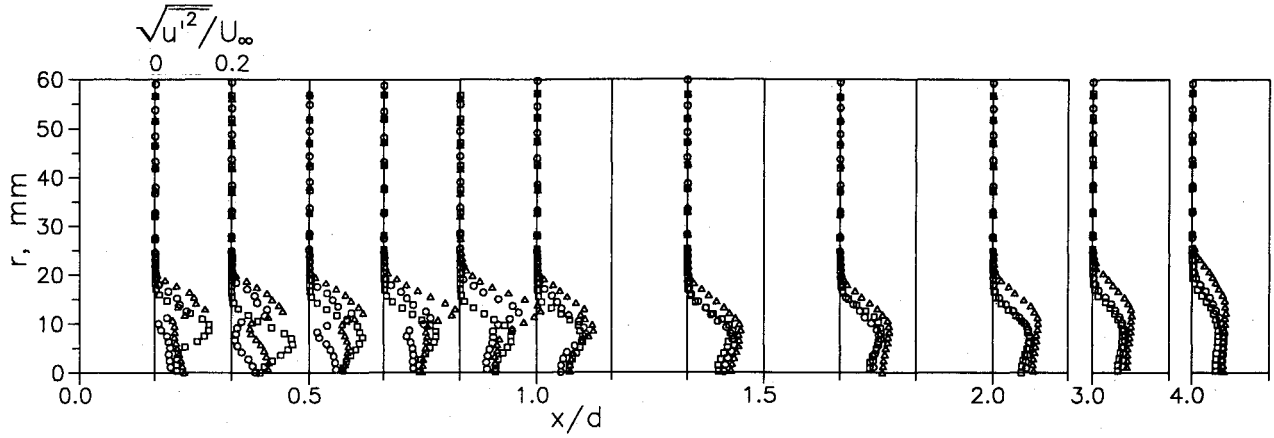

Fig. 6 Turbulence intensity profiles across the wake (Δ: model 1, ○: model 2, □: model 3).

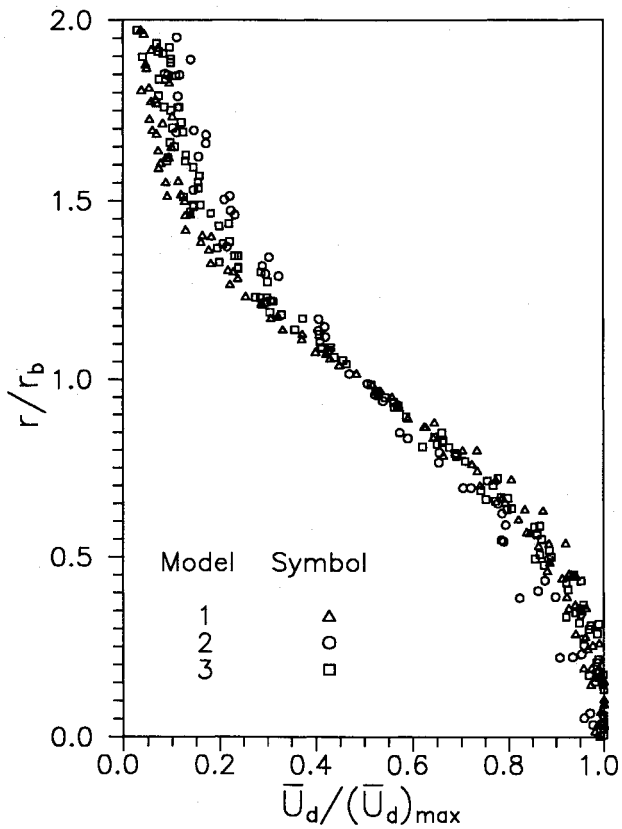

Fig. 7 Far-wake mean velocity similarity profile.

cylindrical surface around the wake centerline, first converging in the near-wake region and then diverging in the far-wake region, and reaches its highest value ($u_0 \cong 0.22$, 0.17, and 0.16 for models 1, 2, and 3, respectively) on a circle around the free-stagnation point. The diameter of this circle is about 0.87, 0.80, and 0.43 times the maximum body diameter for models 1, 2, and 3, respectively. When the mean velocity and turbulence intensity profiles given in Figs. 5 and 6 are considered together for any longitudinal station, it is seen that the peaks on the turbulence velocity profile correspond to the points on which the mean velocity gradient has the maximum values. This fact is due to the enhanced mixing at those points.

The mean velocity profiles in the far-wake region show a similarity for all of the models in the reduced variables of $U_d/(U_d)_{max}$ vs r/r_b, as seen in Fig. 7. A similar figure was given by Merz et al.[4] for an axisymmetric semi-elliptical afterbody.

The drag coefficients of the models obtained by using the mean velocity profiles across the wake at stations of $x/d = 4$ indicate that the drag of model 3 has the lowest value ($C_D = 0.21$), whereas the drag of model 1 ($C_D = 0.42$) is higher than that of model 2 ($C_D = 0.32$), as expected.

Conclusions

The wakes of three axisymmetric bodies with different afterbody geometries, aligned with a uniform freestream, were experimentally investigated at a low subsonic velocity. The major conclusions of this study are as follows:

1) The use of a boat-tail geometry as an afterbody makes the recirculation region shorter and the reverse flow slower.

2) The use of a circular cylinder with a constant diameter instead of a flared geometry reduces the turbulence intensity in the wake. This reduction becomes more pronounced with a boat-tail.

3) The velocity fluctuations become more dominant near the base and near the free-stagnation point.

4) The maximum of turbulence in the wake takes place on a cylindrical surface around the wake centerline, which extends in the freestream direction, first converging in the near-wake region and then diverging in the far-wake region. The maximum turbulence points correspond to the points on which the mean velocity gradient has its maximum values.

5) The mean velocity profiles across the wake in the far-wake region show a similarity for all of the considered models.

6) The use of a circular cylinder with a constant diameter instead of a flared afterbody reduces the total drag. However, a boat-tail is more effective in reducing drag, as expected. Therefore, the boat-tail type afterbody is in general use in the missile industry.

Acknowledgment

This work has been supported by the NATO-AGARD through the Support Project T-70, and DPT (State Planning Organization of Turkey). The authors wish to acknowledge J. Delery of ONERA for his valuable recommendations.

References

[1]Delery, J., and Siriex, M., "Ecoulements de Culot," AGARD-LS-99, March 1979, pp. 6.1-6.78.

[2]Delery, J., and Lacau, R. G., "Prediction of Base-Flows," AGARD-R-754, March 1987, pp. 11.1-11.72.

[3]Merz, R. A., Page, R. H., and Przirembel, C. E. G., "Subsonic Axisymmetric Near-Wake Studies," *AIAA Journal,* Vol. 16, No. 7, 1978, pp. 656-662.

[4]Merz, R. A., Yi, C. H., and Przirembel, C. E. G., "The Subsonic Near-Wake of an Axisymmetric Semielliptical Afterbody," *AIAA Journal,* Vol. 23, No. 10, 1985, pp. 1512-1517.

[5]Atli, V., "Wakes of Four Complex Bodies of Revolution at Zero Angle of Attack," *AIAA Journal,* Vol. 27, No. 6, 1989, pp. 707-711.

[6]Atli, V., "Subsonic Flow over a Two-Dimensional Obstacle Immersed in a Turbulent Boundary Layer on a Flat Surface," *Journal of Wind Engineering and Industrial Aerodynamics,* Vol. 31, Nos. 2-3, 1988, pp. 225-239.

[7]Chevray, R., "The Turbulent Wake of a Body of Revolution," *Journal of Basic Engineering, Transactions of ASME,* Vol. 90, Series D, No. 2, June 1968, pp. 275-284.